Computers and Geosciences 120 (2018) 10–20

Contents lists available at ScienceDirect

Computers and Geosciences

journal homepage: www.elsevier.com/locate/cageo

OpenHVSR - Processing toolkit: Enhanced HVSR processing of distributed microtremor measurements and spatial variation of their informative content

Samuel Bignardi[a,*], Anthony J. Yezzi[a], Simone Fiussello[b], Albert Comelli[a,c,d]

[a] School of Electrical and Computer Engineering, Georgia Institute of Technology, Atlanta, GA, USA
[b] GeoStudioFG, San Colombano Belmonte, TO, Italy
[c] Institute of Molecular Bioimaging and Physiology, National Research Council (IBFM-CNR), Cefalù, PA, Italy
[d] Department of Industrial and Digital Innovation (DIID), University of Palermo, PA, Italy

ARTICLE INFO

Keywords:
HVSR
Processing
2D
3D
Bedrock mapping
Lateral variations

ABSTRACT

The investigation of seismic ambient noise (microtremor) in spectral ratio form, known as the Horizontal-to-Vertical Spectral Ratio technique, is extremely popular nowadays both to investigate large areas in a reduced amount of time, and to leverage a wider choice of low cost equipment. In general, measurements at multiple locations are collected to generate multiple, individual spectral ratio curves. Recently, however, there has been an increasing interest in spatially correlating informative content from different locations. Accordingly, we introduce a new computer program, "OpenHVSR – Processing Toolkit", developed in Matlab (R2015b), specifically engineered to enhance data processing with the purpose of spatially correlating different forms of informative data content, creation of maps, and display of the results in 2D and 3D. The interface is designed to be user friendly while tightly binding processing and visualization so that the effects of different processing choices can be immediately evaluated. Further, bedrock mapping capability, as introduced by Ibs-von Seht and Wohlenberg (1999) is included both through the computation of bedrock depth via a set of published regressions or by computing a customized regression based on the data at hand. The program aims at implementing the most effective and desirable processing tools present in other commercial and non-commercial alternatives, all in one bundle, freely available to the scientific community. In addition to incorporating and enhancing currently available state of the art tools, we have integrated several original features that are not present in any other program. The presented processing toolkit naturally integrates with our data inversion software, "OpenHVSR", published in 2016. Together, they constitute a complete workflow for the Horizontal-to-Vertical Spectral Ratio method. We expect this first version to be of great use to researchers and hope it will constitute the basis for further collaborative development toward future releases oriented at exploring the potentials of this technique.

1. Introduction

The investigation of seismic ambient noise (microtremor) in spectral ratio form, (*i.e.* the ratio between the Fourier spectra of the horizontal and vertical components of motion), as introduced by Nogoshi and Igarashi (1970, 1971) and largely disseminated by Nakamura (1989, 2000), has nowadays become very popular for the investigation of shallow subsurface structure. As outlined by Guéguen et al. (2007), the method is used mainly for three different scientific purposes, namely the evaluation of resonance frequency as correlated to earthquake damage, the investigation of resonance variation over large areas for microzonation and seismic-risk mitigation purposes, and finally the evaluation of sedimentary cover thickness or equivalently, bedrock depth. Applications span a wide variety of scientific disciplines, such as geology (Mantovani et al., 2018), seismology and microzonation studies (Scherbaum et al., 2003; Gallipoli et al., 2004a; D'Amico et al., 2008; Albarello et al., 2011; Mantovani et al., 2015; Paolucci et al., 2015), engineering (Shiono et al., 1979; Mucciarelli and Gallipoli, 2001; Gallipoli et al., 2004b; Gallipoli et al., 2018) and even archaeology (Obradovic et al., 2015; Castellaro et al., 2008; Wilken et al., 2015; Abu Zeid et al., 2016, 2017a; 2017b; Bignardi et al., 2017). A comprehensive description of the concepts and evolution of this technique can be found in (Bard, 1998; Mucciarelli and Gallipoli, 2001; SESAME Project, 2004, 2005; Picozzi et al., 2005; Castellaro and

* Corresponding author. G School of Electrical and Computer Engineering, Georgia Institute of Technology, Atlanta, GA, USA.
E-mail addresses: bgnsml@unife.it, sbignardi3@mail.gatech.edu (S. Bignardi).

https://doi.org/10.1016/j.cageo.2018.07.006
Received 30 December 2017; Received in revised form 12 April 2018; Accepted 19 July 2018
Available online 20 July 2018
0098-3004/ © 2018 Elsevier Ltd. All rights reserved.

Mulargia, 2009; D'Alessandro et al., 2016). Its widespread popularity stems from measurements performed in a matter of minutes with just one operator and low cost equipment.

The core of the method revolves around the computation of the so-called "horizontal-to-vertical spectral ratio" curve (HVSR or H/V). Typically, a three-component seismic record is split into several windows of pre-defined length. For each data window the Fourier spectra of all components are computed, properly smoothed, and the ratio between a combination of the horizontals over the vertical component is obtained. From now on, we will refer to the east, north, and vertical components of motion as E, N and V respectively. It should be clear from the context when we are referring to the recorded microtremor versus its Fourier transform. The average horizontal spectrum, as defined in the following, will be indicated with "H" while spectral ratios will be indicated as H/V, E/V and N/V.

The process produces a number of spectral ratio curves equal to the number of original time windows, from which the average spectral ratio (the HVSR-curve) as a function of frequency, as well as the corresponding error, are then computed. Since the method is focused on processing natural seismic noise, data windows which contain transient signals should be discarded. We will refer to the action of selecting a group of windows (either to be included or excluded from further processing) as "window selection", while we will refer to the action of excluding some windows from further processing as "data cleaning".

Currently available processing software includes some open source codes, such as "Sesame" created during the homonymous project (SESAME Project, 2004), and its subsequent extension "Geopsy" (http://www.geopsy.org, Wathelet et al., 2004, Wathelet, 2008). Among commercially distributed packages, "Grilla" (http://moho.world) is probably the most popular, closely followed by software products from "SARA electronic instruments s.r.l" (http://www.sara.pg.it/) and "Geogiga Technology corp." (www.geogiga.com). While detailed analysis of existing software products is beyond the scope of this paper, it is important to note that each mentioned software package offers desirable features, especially regarding the critical data cleaning operation. Geopsy, for example, plots the HVSR curve for each window in the same graph so that anomalous-looking curves can be easily recognized and discarded before the average is computed. Grilla, on the other hand, tiles HVSR curves side-by-side in time-frequency view, so that discontinuities in peaks across time are highlighted. As HVSR surveys typically involve the processing of multiple measurements, Geopsy can save and reuse the processing parameters while Grilla actually handles all the measurements in the same interface.

Concerning the HVSR curve, it is now well understood that when the subsurface can be represented by a stack of sedimentary layers residing on hard bedrock, the HVSR curve will exhibit one or more peaks. A long debate has driven the growth in understanding the origin of such peaks. In the early 1970s several Japanese scientists (Nogoshi and Igarashi, 1971; Shiono et al., 1979; Kobayashi, 1980) assessed the physical significance of the HVSR showing its direct relationship with the ellipticity of Rayleigh waves. On the other hand, in 1989, Nakamura, explained HVSR peaks as the result of multiple reflections of vertically incident body waves. Finally, in 2000, Nakamura generalized the theory showing that both contributions from surface and body waves may affect the shape of the curve in variable proportions depending on the subsurface visco-elastic properties, distance, and distribution of sources (Bonnefoy-Claudet et al., 2006). More recently, considerable effort has been devoted to understanding the connection between the intimate nature of the wavefield and the HVSR (Bonnefoy-Claudet et al., 2006, 2008; Lunedei and Albarello, 2010, 2015; Sánchez-Sesma et al., 2011; Matsushima et al., 2014). While, on the one hand, it is impossible to discriminate to what extent body waves and surface waves (with their different propagation modes) are present in microtremor, it seems, on the other hand, quite established that the HVSR curve will present local maxima at the resonance frequency of the S waves regardless of the nature of the wavefield (Albarello and Castellaro, 2011). In general, when multiple peaks are present, the significant peak with lowest frequency is sought associated with the fundamental resonance frequency (f_0) of the sedimentary cover. Criteria to define a significant peak were established in SESAME (2004) and successively integrated by Albarello and Castellaro (2011).

Further, Castellaro and Mulargia (2009) showed that comparison of the smoothed spectra E, N and V may be used to discern whether a peak possess stratigraphic origin or whether the presence of velocity inversion should be investigated instead.

The HVSR method exhibits two different levels of sophistication. At the processing level, the HVSR curve is used to infer the main resonance frequency of a site and to evaluate the presence of directional effects in the data. At a higher level, the HVSR curve can be inverted to infer the visco-elastic properties of the subsurface (Ben-Menahem and Singh, 1981; Tsai and Housner, 1970, Aki and Richards, 2002; Sánchez-Sesma et al., 2011; Lunedei and Albarello, 2010, 2015). Numerical inversion generates subsurface velocity models for seismic, geotechnical, and engineering applications, therefore, most modern software packages implement inversion routines for the HVSR curve. In this context, Bignardi et al. (2016) published the open source computer program "OpenHVSR" for the inversion of datasets containing a large number of HVSR curves in order to generate 2D and 3D subsurface models.

Indeed, since data acquisition is so flexible, the typical HVSR survey often consists of a multitude of measurements extracted from different locations over an investigated area. Availability of such datasets has triggered a new perspective on HVSR surveys, where the informative data content is treated as spatially varying. This is further motivated by the fact that lateral variation may heavily impact wave propagation, especially for surface waves (Guéguen et al., 2007; Bignardi et al., 2013, 2014; Matsushima et al., 2014; Bignardi, 2017). The work of Bignardi et al. (2016, 2018) aimed to create an inversion tool following this new perspective.

However, quality information can be extracted from the data even at the processing level, for example, the map of the main resonant frequency on the investigated area represents a good indication of subsurface morphology. Additional typical examples from this perspective include "HVSR profiling" (Herak, 2008; Herak et al., 2010), which produces a tiled view of HVSR curves and transforms the vertical axis from frequency into "pseudo-depth" using an approximated average velocity of the soft sedimentary stack, as well as "bedrock mapping" introduced by Ibs-von Seht and Wohlenberg (1999) and further investigated by (Delgado et al., 2000; Parolai et al., 2002; Gosar and Lenart, 2010; Hinzen et al., 2004; Garcia-Jerez et al., 2006; Motamed et al., 2007; D'Amico et al., 2004; Abu Zeid et al., 2014; Bignardi, 2017).

The creation of maps to describe the variation of f_0 across the surveyed area is typically performed after the data processing phase (with standard tools) is concluded. This typically consists of manually extracting the main resonance frequency of each HVSR curve to create an organized list of points which are then interpolated into a surface and displayed. In the case of bedrock mapping, a functional relationship of the form $h = af_0^b$ is established to relate f_0 obtained from the measurements corresponding to excavated wells, to the known bedrock depth h. The inferred parameters a and b are then used to compute the depth at the remaining locations. In both cases this workflow is often tedious and time consuming. Further, since the mapping is performed after HVSR curves are obtained, there is no possibility of verifying how processing parameters affected the result. As a final note, this workflow prevents the investigation of data features that are available only at the processing level, and any change in the processing parameters requires the researcher to start over.

This motivated us to create a new computer program, developed in Matlab (R2015b), which we have named "OpenHVSR-Processing Toolkit". In contrast to our previous program "OpenHVSR" (Bignardi et al., 2016), which was entirely devoted to the inversion of HVSR curves already provided by the user, this new software is dedicated to

the generation, as well subsequent user-interaction and display, of HSRV curves directly from raw field data. It has been engineered to enhance such processing, with the purpose of spatially correlating different forms of informative data content (e.g. main resonant frequency, main peak amplitude, the signal's preferential arrival direction), to create geospatially referenced HVSR maps, perform preliminary bedrock mapping, and to display the results in 2D and 3D. All data are loaded into the same environment, and a choice of processing parameters can be immediately applied to all of the data, thereby minimizing the amount of manual work. The interface is designed to be user friendly while tightly binding processing and visualization so that the effects of different processing parameters choices can be immediately evaluated. In addition, bedrock mapping capability is included both through the computation of bedrock depth via a set of published regression constants or by customized regression using the data at hand.

The program aims at implementing the most effective and desirable tools present in other commercial and non-commercial alternatives, all in one bundle, freely available to the scientific community.

We expect this first version to be of great use to researchers and hope it will constitute the basis for further collaborative development toward future releases oriented at exploring the potentials of the HVSR technique.

In what follows, the main features of OpenHVSR – Processing Toolkit will be introduced. The images will not only show the appearance of the program's user interface, but will also illustrate some of the processing capabilities on an example microtremor dataset taken from a hydro-geological survey at the Serravalle Sesia sedimentary basin (Italy), where measurements from 19 different sites were performed. Further examples on the processing of the field data will be shown in the last section of this paper.

2. Algorithm and features

The algorithm is composed of several routines integrated into a main graphical user interface (GUI) organized in tabs.

Most of the input/output functionality is managed through the scroll down menu labelled “Files”. The input consists of a text project file, either created using the program's dedicated graphical interface or manually edited, which specifies the field geometry (i.e. locations of measurements, including elevation), data path and filenames, an optional path to files describing topography, and an optional path to files containing lito-stratigraphic description of local wells. To allow the user maximum flexibility, the field data files may contain any number of columns (channels) in any order in ASCII text format with any optional header content. Microtremor data files in “*.saf” format (SESAME project, version 1.0) are automatically managed without any intervention by the user. In this case, all necessary information, such as data column ordering and sampling frequency are automatically retrieved from the file header. Some variations of the standard *.saf format, such as those generated using MAE (http://www.mae-srl.it/), Tromino (http://www.tromino.it), and Pasi (http://www.pasisrl.it) instruments, are automatically managed as well.

A mixture of different file structures is also allowed, including different record lengths and different sampling frequencies. By default, we assume the data have north and east components oriented toward the geographic north and east respectively. Otherwise, the user may specify a rotation angle. This option is location specific so that a mixture of data acquired with different instrument orientations is possible.

The GUI is structured into six tabs. Tabs 1–3 are devoted to signal processing and data cleaning. Tabs 4 and 5 are devoted to visualization, while Tab 6 is devoted to bedrock mapping. In what follows, we will describe the main features of this new program. The interested reader should refer to the color images on the online version of this paper. Further detailed information can also be found in the user manual distributed with the toolkit.

Tab 1, “Main” (Fig. 1) is dedicated to the general view of the survey. The top-right panel (a) shows an aerial view of the survey including measurement locations, optional topographic points, and existing wells. The location corresponding to the data undergoing processing is highlighted by a red circle, while user-defined profiles used in subsequent tabs to display HVSR-profiling images, are shown with red lines. The top part of left panel (b) hosts controls for navigating through different locations and wells, to switch to “profile-view” mode (when linear profiles are defined), to navigate through the profiles, and to inspect which recording stations are included. Measuring stations can be selectively included or excluded from any profile by using the “add” and “remove” buttons respectively. The capability of defining multiple profiles and manually modifying them by including/excluding single stations represent two new extended enhancements over original HVSR profiling (Herak et al., 2010). Panel (b) also displays basic information regarding the highlighted measurement being considered for processing as well as the corresponding processing parameters (lower section, d). The associated data filename is shown in panel (d). For the sake of clarity, the reference system internally adopted by the program is superimposed on the top-right figure within panel (a).

Tab 2, “Windowing” (Fig. 2) is devoted to data windowing and splitting. A smaller aerial view from Tab 1 is replicated in the top-left panel (a) together with the filename, while the bottom-left panel (b) contains the subset of processing parameters specific to the windowing operation, such as the window's width, overlap percentage, short-to-long term average amplitude parameters for the STA/LTA ratio (Withers et al., 1998), and digital filter options. The user can customize the windowing operation by using these controls.

The parameters can be used either for the displayed data or the entire dataset in batch mode. Within the right panel (c), the three components of motion are shown along with the time windows. Active windows are displayed in color, while discarded windows are white. Selection of time windows (to either be enabled or discarded) as well as visualization customization can be performed by right-clicking on the figure axes. Additional data window selection options are available in Tab 3.

Tab 3, “Computations” (Fig. 3), follows the same layout as Tab 2, with the survey map, currently visualized data filename, and navigation controls replicated on the top-left panel (a). Controls for selecting the HVSR processing parameters lie within the bottom-left panel (b) and include the strategy to combine the horizontal components when computing the spectral ratio, the frequency range of interest (in Hz), the window's cosine tapering percentage, zero-padding, and smoothing preferences.

In detail, the selector labelled “HVSR” on top of panel (b) controls the formula to be used for the horizontal component of the spectral ratio H/V. Available options are:

$$\text{Average squared (RMS): } H(f) = \sqrt{\frac{E(f)^2 + N(f)^2}{2}} \tag{1a}$$

$$\text{Simple Average: } H(f) = \frac{E(f) + N(f)}{2} \tag{1b}$$

$$\text{Total energy: } H(f) = \sqrt{E(f)^2 + N(f)^2} \tag{1c}$$

Cosine tapering multiplies the beginning and ending parts of the data windows by a cosine function to make the data amplitude fade to zero toward the edges of the window. The tapering value is expressed as a percentage of the window's length.

Zero-padding refers to the action of adding zero valued samples to each window in order to increase the spectral resolution in the frequency domain.

Finally, horizontal and vertical spectra are smoothed before computation of the spectral ratio. Available smoothing options are the Konno and Ohmachi method (1998) or a moving average.

The same panel (b) hosts the controls for the directional analysis of the spectral ratios. This feature, switched off by default, is enabled

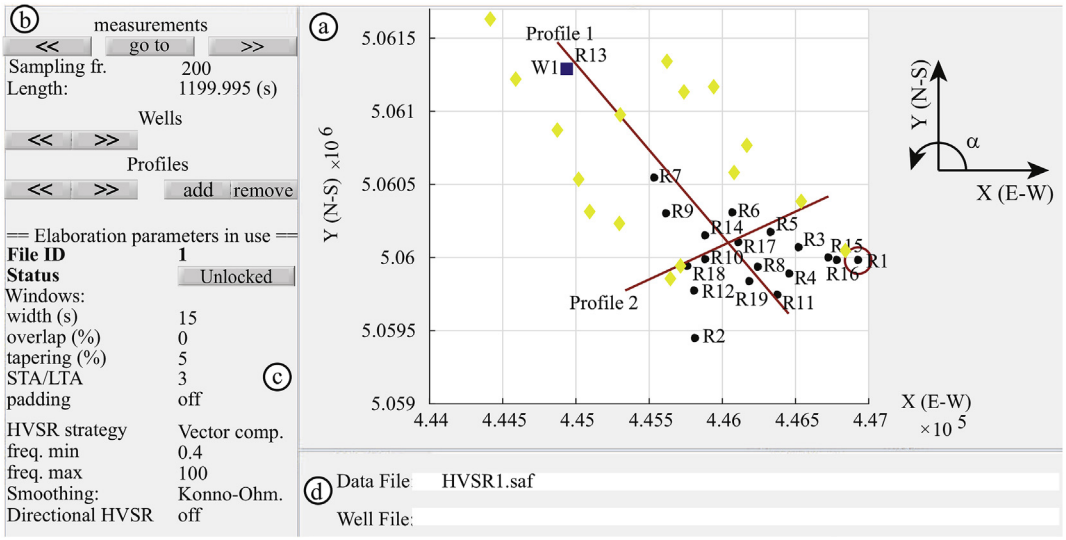

Fig. 1. The "Main" tab. Panel (a) provides an aerial view of the survey, including measurement locations (black dots), optional topographical points (yellow diamonds), wells (blue squares), and line profiles defined by the user (red lines). Panel (b) contains controls for navigation across different objects of the main view while processing parameters applied to the data currently highlighted (red circle) are shown in panel (c). Panel (d) shows the file names for the currently highlighted recording station and well. (For interpretation of the references to color in this figure legend, the reader is referred to the Web version of this article.)

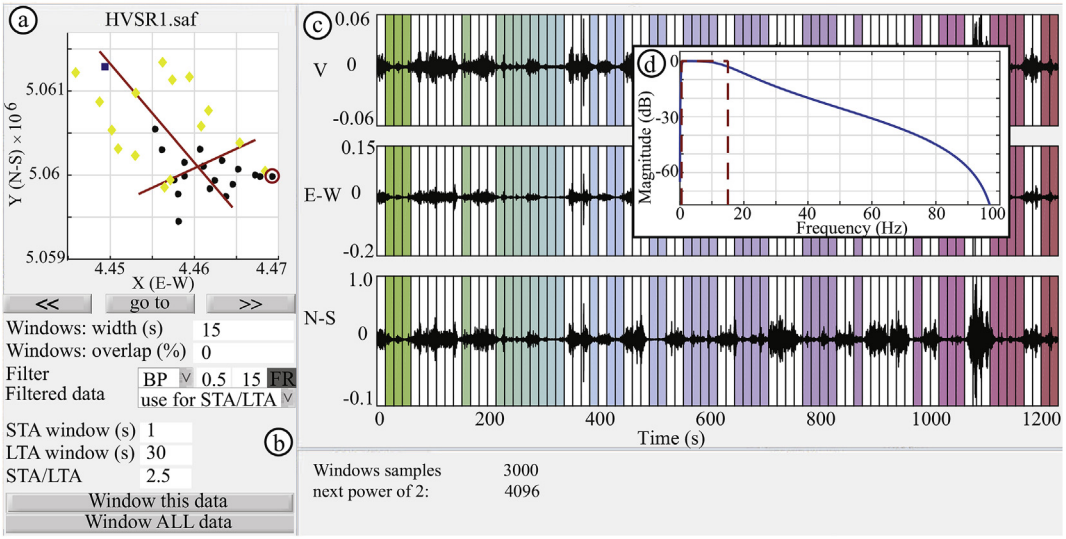

Fig. 2. The "Windowing" tab, devoted to data splitting. Panel (a) shows an aerial view of the survey highlighting the currently displayed data and the corresponding filename. Panel (b) groups the parameters for data splitting and navigation controls, while panel (c) shows the three components of motion along with the selected time windows. (d) example of Band-Pass filter magnitude response.

when the user selects a value in the "angular sampling" control. The horizontal components of motion, E and N, oriented according to the axis of our reference system (X, Y), are projected onto a rotated system of axis (X′, Y′). The horizontal component along the X′ direction, H_α, is then used to compute the directional spectral ratio H_α/V, where α is the angle between the X and X' axis (see the reference system in Fig. 1). Spectral ratio curves for angles between 0 and 180° are computed for different angle steps to investigate whether data contain directionally-dependent (i.e. non-isotropic) components (Barazza et al., 2009). Directional spectral ratios are tiled to form the columns of a matrix $\boldsymbol{R}$ so that different rows (m) and columns (n) correspond to different values of frequency (f_m) and angular direction (α_n) respectively. The matrix $\boldsymbol{R}$ as described in the following, is displayed on the interface and labelled "HVSR-Directional". Users familiar with Geopsy will recognize the general design the HVSR-rotate tool.

We further enhance directional analysis by introducing the "preferential signal arrival vector". For each row m of the $\boldsymbol{R}$ matrix (i.e. each frequency f_m), the maximum amplitude in the row $r_{max} = max_n(R^{mn})$, its corresponding column index n^*, and the angular direction $\alpha(n^*)$ are extracted along with the average row-amplitude $r_{mean} = mean_n(R^{mn})$. Ideally, if no directional effect is present, it is expected that

$$|r_{max} - r_{mean}| = 0.$$

Therefore, for each row m of matrix R we build a 2D vector $\boldsymbol{V}(f_m)$ in the $\alpha(n^*)$ direction with modulus $V = |r_{max} - r_{mean}|$. Finally, each station of the survey will be associated with a directional analysis matrix $\boldsymbol{R}(f, \alpha)$ and frequency-dependent preferential direction of signal arrival $\boldsymbol{V}(f)$ displayed in the subsequent tabs 4 and 5

As in the previous tab, the parameters can be used either for the data currently being processed or for the entire dataset. Panel (c), on the top-right, is used to display various visualizations selected in the bottom-right panel (d).

Available visualizations include:

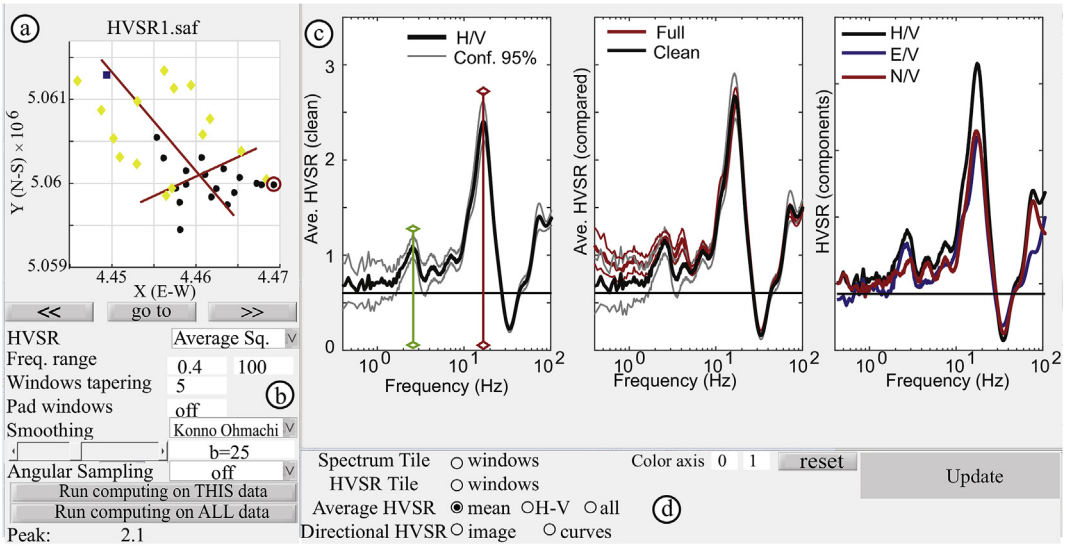

Fig. 3. The "Computations" tab, devoted to signal processing. Panel (a) shows an aerial view of the survey highlighting the currently displayed data and the corresponding filename. Panel (b) groups the parameters for data processing and navigation controls, while panel (c) hosts the visualization section. User can choose between seven visualization modes, selected by using the radio buttons placed on panel (d).

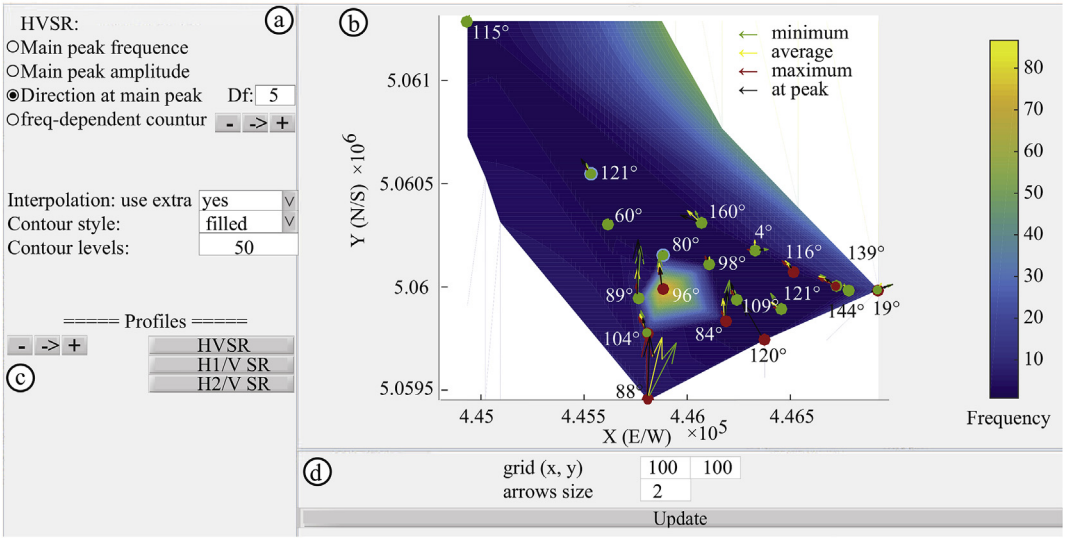

Fig. 4. The "2D Views" tab: Panel (a) host the control to plot different informative contents which are shown in panel (b) as a geo-referenced interpolated map. Controls (c) are used to plot the linear profiles (if defined by the user), obtained by interpolating the spectral ratios for selected subset of stations.

1 Tiled view of window spectra: Vertical, East, and North components are shown within the left, central and right axes respectively. Pixel images and contour plots are available. Horizontal and vertical ranges may be customized to zoom in and better investigate the details of the image. To our knowledge, this mode is not present in other software packages and enables window selection based on spectral investigation of any motion component.

2 Tiled view of window HVSR's: It implements a display strategy similar to the Grilla program, but with an enhanced window selection strategy allowing the user to investigate both N/V, and E/V spectral ratios along with the classic HVSR. Standard visualization modes and zooming features are also available.

3 Average HVSR (via "mean" option): The final average curve and 95% confidence intervals are displayed within the left plot. Mean curves and confidence before and after data-cleaning are shown in the center to allow the user to investigate both the impact of different parameter choices and the effectiveness of the data cleaning operation. The HVSR curve, labelled H/V, and the mean curves for the ratios E/V, and N/V are compared within the right plot. In this view the user may right-click on the left plot axes to open the figure's context menu and select "Use Manual Peak" option to perform the manual selection of the fundamental mode peak.

4 Average HVSR (via "H-V" option): The same left and right plots described above are shown. With this option, however, the central plot shows a comparison of the smoothed East, North and Vertical spectra in order to investigate whether the peaks have lithological origin or whether the data show evidence of elastic impedance inversion in the subsurface (Castellaro and Mulargia, 2009).

5 Average HVSR (via "all" option): Shows the spectral ratio for all windows associated with the investigated station. HVSR is displayed (as in Geopsy) within the left plot, while the E/V and N/V ratios are shown within the central and right plots respectively. This mode accommodates window selection through user highlighting of anomalous curve segments within any of the three plots.

6 Directional HVSR (via "image" option): The directional analysis matrix R is displayed via contour plots. On the left the image it is

shown not normalized, while frequency and angle-wise normalizations, are displayed in the central and right axes respectively. The average HVSR curve and the line corresponding to unit amplitude of the spectral ratio are superimposed for legibility sake.

7 Directional HVSR (via "curves" option): The directional analysis matrix R is displayed as a contour plot on the left, while the central plot contains the HVSR curves computed at each angle step as frequency-amplitude graphs. (no plot appears on the right in this case).

Tab 4, "2D Views" (Fig. 4), is dedicated to aerial map visualizations (panel b). Filled and unfilled colored contour plots of the investigated area are used to image the spatial distribution of

- resonant frequency values (f_0)
- amplitude at the resonant peak
- preferential direction of incoming waves (i.e. vector $\boldsymbol{V}(f)$): The values at the peak $\boldsymbol{V}(f_0)$ and the maximum and minimum angular directions computed for a frequency buffer df centered around f_0 are shown.
- navigable frequency dependent amplitude pattern

Which are selected operating the controls on panel (a), while panel (c) hosts the controls for the visualization of linear profiles.

Tab 5, "3D Views" (Fig. 5), is devoted to displaying processing results in three dimensions in order to visually facilitate their interpretation. Options available include:

- plot of the resonant frequency ($z = 1/f_0$), as function of spatial coordinates X (E/W) and Y (N/S) to gain insight into the bedrock morphology across the area.
- plot of the resonant frequency as function of spatial coordinates X and Y, with preferential direction $\boldsymbol{V}(f_0)$ attached to the data points to investigate whether or not a connection between bedrock geometry and directional contributions exists. A frequency buffer df centered on f_0 can be investigated as well.

Preferential direction of signal arrival $\boldsymbol{V}(f)$ as a function of frequency (one curve at a time). The x (E/W) and y (N/S) components of the preferential direction and corresponding frequencies are displayed along the X, Y and Z axes respectively, directions of interest are displayed through lines whose lengths represent how much the spectral ratios at each frequency-direction pair (f_m, θ) exceed the average ratio at frequency f_m.

It is worth mentioning that one of the purposes of the program is to speed up the creation of geo-referenced maps. Images on the interface are meant for quick visualization purpose and therefore, a simple linear interpolation approach is used. For enhanced geological interpretation (e.g. Agostini et al., 2015), we advise exporting any final results to third party software packages with more sophisticated interpolation capabilities.

Tab 6, "IS&W", is named from an acronym that refers to the bedrock mapping method introduced by Ibs-von Seht and Wohlemberg (1999). In this tab, the bedrock depth, obtained using different regression laws available in the literature, is shown using a set of color coded points placed under the measurement points (Fig. 6d). A topographic surface of the terrain is produced using the coordinates of the measurement points and, if available, the points input by the user. Bedrock surfaces obtained by different regression laws can be simultaneously or individually plotted to build a comprehensive view of the sedimentary system. Further, if either a sufficient set of well files are included in the project or the user manually specifies the bedrock depth at a sufficient number of locations, a custom regression is computed (Fig. 6c). The corresponding bedrock depth estimates and reconstructed geometry can be shown as well.

3. Other general features

The program can generate different forms of output. The main processing results are the HVSR curves, which can be exported as ASCII files with extension "*.hv".

All figures displayed on the interface can be opened within standalone windows, where the power of Matlab's graphical tools may be used to fully customize their final appearance.

All data internally produced during computation can be exported as text-files to be reused with third-party software. For example, bedrock maps can be exported for later use in GIS, where they can be integrated with a suitable Digital Elevation Model (DEM) (Bignardi et al., 2018). A system of headers embedded within the exported files offers a straightforward description of their content.

Further, the status of the data processing can be saved at any time and resumed when needed. As a final remark, HVSR curves can be exported along with a starting guess for the subsurface model in form of an OpenHVSR project-file (Bignardi et al., 2016) for subsequent inversion (not discussed in this paper).

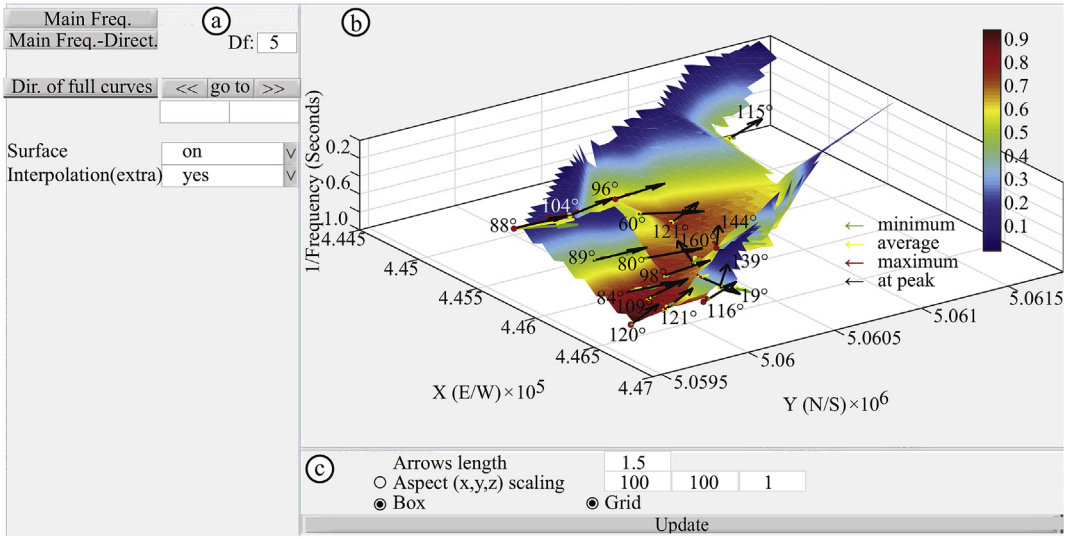

Fig. 5. The "3D views" tab, displays different data properties in three dimensions. The resonant frequency may be used to visualize a linearly interpolated surface representative of the bedrock's morphology. Interpolation may take advantage of additive topographical points which the user can optionally supply.

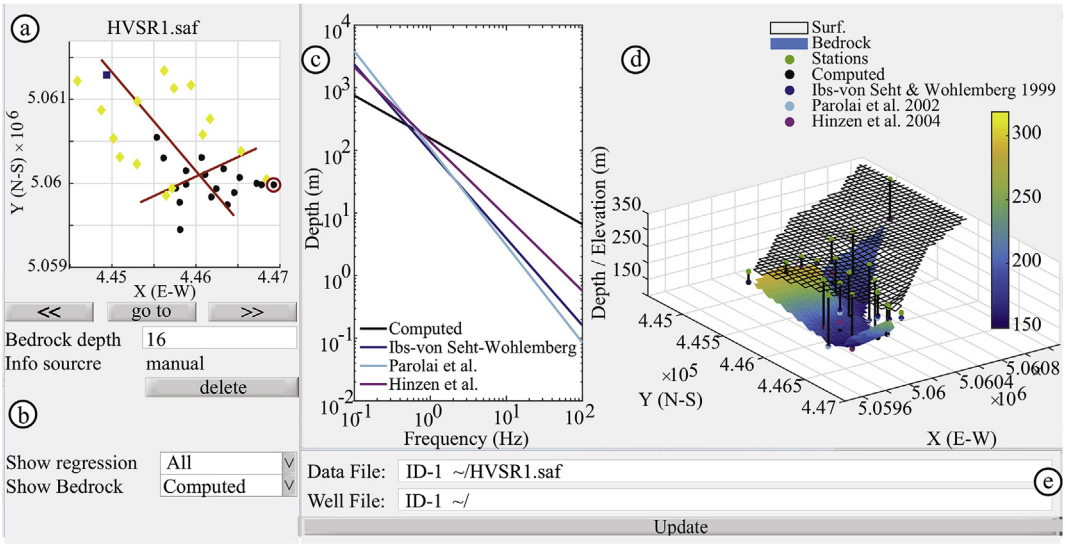

Fig. 6. The "IVS&W" tab, named after Ibs-von Seht & Wohlemberg. Panel (a) shows an aerial view of the survey highlighting the currently displayed data and the corresponding filename. Panel (b) displays information on the bedrock depth for the specific measurement, hosts navigation controls, and visualization options. Plot (c) shows different frequency-bedrock depth regressions available in the literature as compared to the one computed for the survey at hand (if available), while plot (d) displays a three dimensional view of topography, an interpolated surface representing the bedrock depth for one selected regression law, and depths estimates corresponding to different regression law (color-coded points). (For interpretation of the references to color in this figure legend, the reader is referred to the Web version of this article.)

4. Example of processing and results

In the broader context of a hydro-geological survey at the Serravalle Sesia sedimentary basin (Italy), which was performed to optimize the exploitation of hydrological resources, we decided to use the HVSR technique to gain insight into the subsurface elastic properties and, in particular, to estimate the bedrock depth. A survey with measurements from 19 different sites was performed. Measurement locations and a set of additional topographical points, used to better constrain the valley geometry, are shown in panel (b) of Fig. 1. Figures 7to 9 show an example of processing results that can be obtained using this program.

Fig. 7 shows the processing results for one selected location in our dataset (highlighted by the red circle in Fig. 1). Fig. 7a, shows how the three components of motion are windowed and how the splitting is graphically represented. Fig. 7b shows a tiled view of all the Fourier spectra of the windows, while a tiled view of the spectral ratios is shown in Fig. 7c. In Fig. 7a, b, and 7c, active and discarded windows are highlighted. Fig. 7d shows the average HVSR curve, along with the computed error, the comparison between clean and unclean spectral ratios, and the comparison between the HVSR obtained by using only one horizontal component at a time. The red and green vertical lines highlight the automatic and manual peak selection respectively. Finally, Fig. 7e shows the spectral ratios of the windows all in one graph. It is worth noting that our program allows window selection within any of the views represented by Fig. 7a, b, 7c and 7e, thus offering the user a wide set of tools for the data cleaning operation. Fig. 8 shows an example of HVSR profiling.

Fig. 9a shows the directional analysis matrix **R**, obtained by rotating the two components of motion and then computing the HVSR, for each angle step (every 1° in the present case), between 0 and 180°. For better interpretation of the results, the program superimposes the average HVSR curve, the mean peak frequency (horizontal) line, and the unit-amplitude (vertical) line onto the color image representing **R**, in order to highlight the frequency ranges where the spectral ratio falls below one (Castellaro and Mulargia, 2009). A plot of all HVSR curves for each angle step is shown in Fig. 9b. It can be seen in this visualization that HVSR curves stack together, producing a line that is wider when a directional dependence is present. It is worth noting in this case that the curve stack is thin at the resonant frequency, which means that the wavefield contributing to the peak is isotropic.

Fig. 9c, shows an example of 3D bedrock mapping (colored surface) obtained using the Ibs-von Seht and Wohlenberg strategy. The use of different regressions will naturally lead to slightly different depth estimations (color-coded points). Thus, when the information about the true bedrock depth is insufficient, this tool should only be used to gain a rough understanding of the bedrock geometry. In such cases data inversion is recommended.

Finally, Fig. 9d shows an example of three dimensional representation of the bedrock built after exporting the results to GIS, and with the local DEM superimposed. With the exception of Fig. 9c, all figures were exported directly from our program.

5. Conclusions

We introduced a new computer program "OpenHVSR - Processing Toolkit" specifically engineered to perform HVSR processing on large microtremor datasets, with the purpose of spatially correlating different forms of informative data content, geo-referenced map creation, and visualization of the results in 2D and 3D.

The strongest point of this program is that processing and visualization are tightly bound so that every processing parameter change (which may be selected differently for each location) is immediately displayed in the refreshed result. This makes the interface user friendly and extremely interactive. In the typical workflow for map creation, the computed HVSR curves must be saved to one or more file before feature extraction and visualization can be carried out in other software packages. With this approach the possibility of extracting and visualizing any intermediate processing byproduct is lost. Furthermore, the whole workflow is often time consuming as it involves the use of several software packages and since changing any processing parameter would require the researcher to start over. Our program performs processing as well as figures, map creation, and data volume visualization all in the same software environment. Changing any parameter will immediately update the final result while all processing information still resides in memory, allowing richer exploration possibilities which other programs do not support. This makes an entire new set of interactive visualization tools available, enabling the user to gain a deeper insight into the informative content of the data, and facilities the integration of new

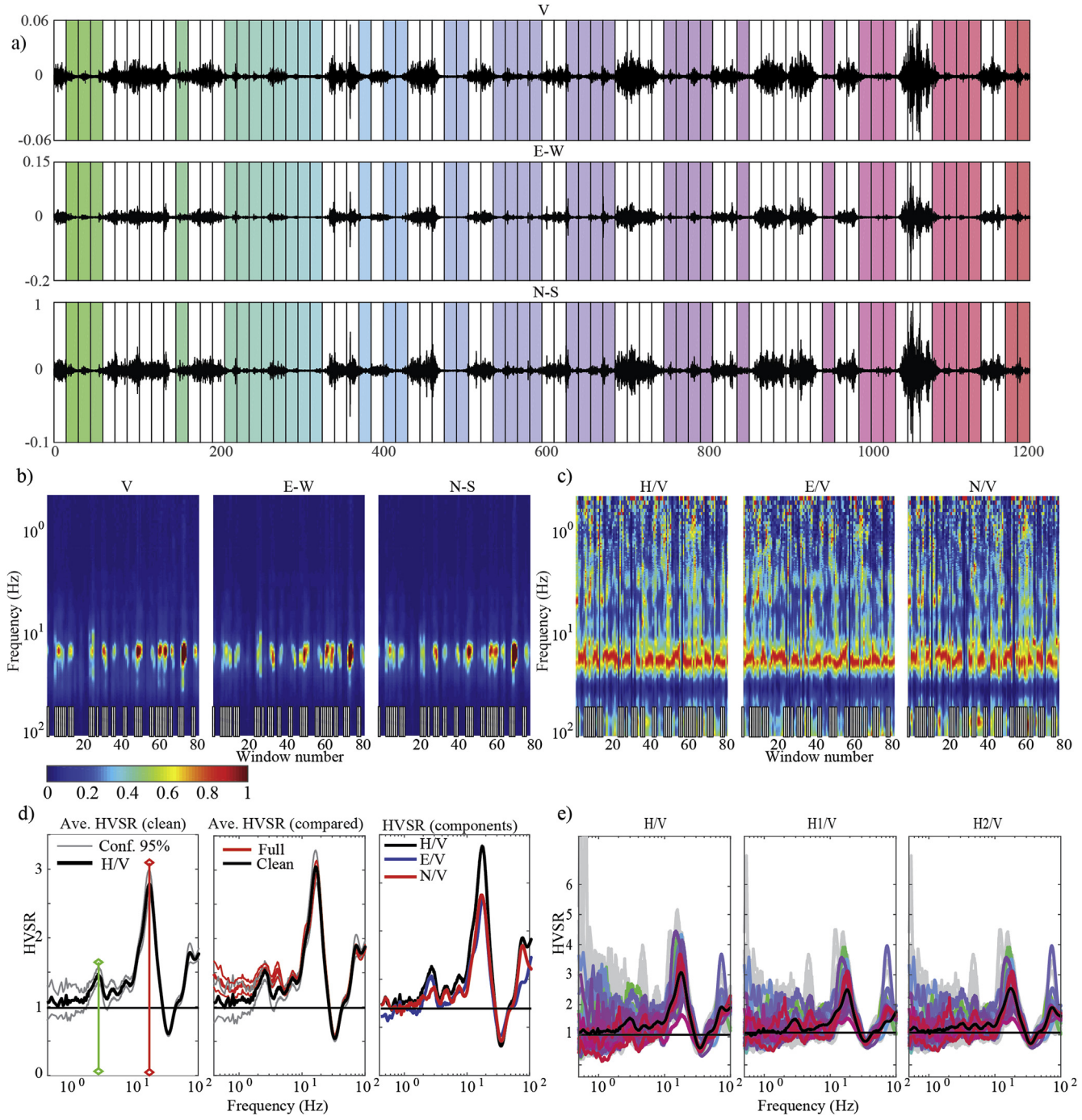

Fig. 7. Selected example of processing result for a microtremor measurement: (a) windowing. (b) tiled view of normalized Fourier spectra. (c) tiled view of normalized spectral ratios. For sake of clarity, data selected windows are highlighted at bottom in figures b and c. (d) average HVSR curve (left), comparison of HVSR curves before and after data cleaning (center), H/V compared to average E/V and N/V ratios (right). (e) HVSR curves for all windows in single plots; H/V, E/V and N/V are shown from left to right.

investigation tools in the future.

In addition to incorporating and enhancing currently available state of the art tools in this field, we have integrated several original features that are not present in any other program. Original features include:

- tiled view of the Fourier spectrum of windows and the capability of window selection in this view
- tiled view of the spectral ratio of windows not only for the *H/V*, but also for the ratios E/V, N/V for the single horizontal component (capability of window selection in this view as well)
- comparison of mean HVSR's before and after data cleaning
- comparison of the ratios H/V, E/V and N/V
- average HVSR curve superimposed over the directional analysis image and visualization with three different normalization strategies
- directional analysis angle increments as small as 1°
- visualization of all directional HVSRs in one window
- automatic map creation for the resonant frequency, amplitude, and preferential signal arrival vector $\boldsymbol{V}(f)$
- use of the HVSR profiler (Herak, 2008; Herak et al., 2010) by defining multiple linear profiles rather than only one, and plots for E/V and N/V as well as the classic HVSR.

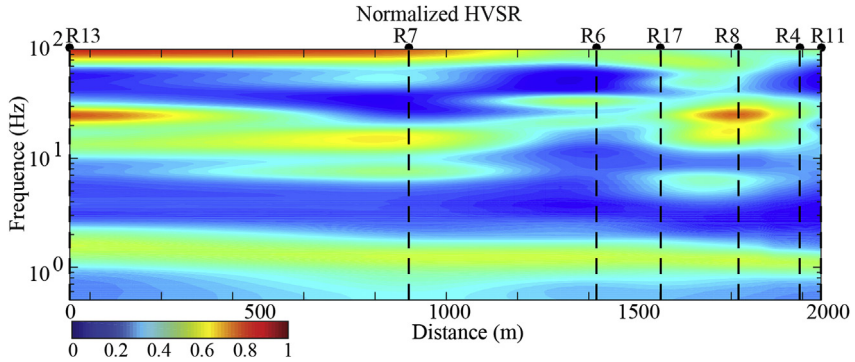

Fig. 8. Example of HVSR profiling for the "profile 1" highlighted in Fig. 1. The normalized spectral ratio is shown as a function of the distance from receiver R13. Topography is not accounted for.

- frequency dependent plot of the HVSR amplitude
- 3D visualization of bedrock morphology, where $z = 1/f_0$, including the preferential signal propagation direction
- for each measurement, the visualization of the preferential signal propagation direction as a function of frequency
- capability of including topography for a better geometric reconstruction
- integrated bedrock mapping using the Ibs-von Seht and Wohlenberg method with the use of multiple regression laws and, when feasible, automatic computation of a custom regression

In the second section of this paper we showed example images from processing a dataset consisting of 19 microtremor measurements. As a result of operating at the processing level with a tool specifically engineered to extract different forms of spatially varying information, a deeper understanding the data is possible. Other properties beyond f_0 can be extracted. Processing and map production speed is dramatically improved. After the input project-file was created, our preliminary 3D bedrock model, based on regression, was produced in minutes and ready to be exported to GIS without further tedious manual work. In addition, these processing results with "OpenHVSR processing toolkit" were readily exported to OpenHVSR for inversion (Bignardi et al., 2018).

Authorship statement

Samuel Bignardi: Original idea and main scientific investigator, code development, code maintenance, GUI design, manuscript composition and revision. Anthony Yezzi: Scientific advising, code testing, manuscript composition and revision. Simone Fiussello: Field data acquisition, data processing with third party software for comparison purposes, results and DEM fusion in the GIS environment. Albert Comelli: Implementation of statistical aspects, code testing, manuscript revision.

Computer code availability

The program "OpenHVSR – Processing toolkit" is an application developed under Matlab (Version, 2015b). It is intended to be Open source and available by contacting the authors, or alternatively downloadable at the internet address https://github.com/sedysen.

Acknowledgments

Part of this work has been supported by NSF Grant CCF-1526848.

Authors would like thanks the GeoStudio FG (www.geostudiofg.it) for permission to use the field data.

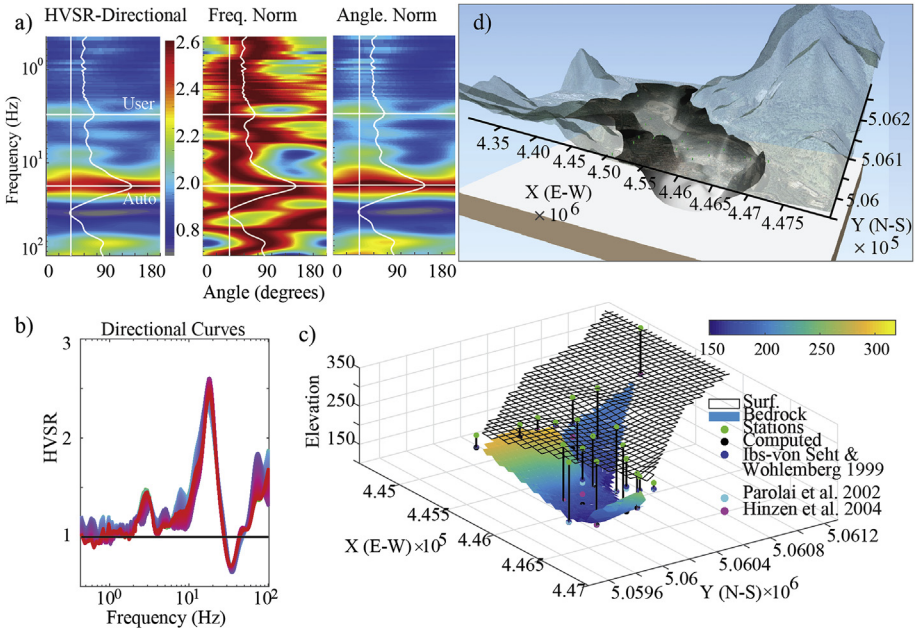

Fig. 9. (a) Directional spectral ratio analysis (**R** matrix). Non-normalized view, Frequency-wise, and angle-wise normalization are shown from left to right respectively. Color represent amplitude as function of frequency and direction. For legibility the average HVSR is superimposed (b) Frequency-amplitude plot view of HVSR curves of image in (a). (c) bedrock depth estimates obtained by different regression laws. The estimate customized on the present dataset is shown as a colored surface. (d) example of bedrock map and DEM fusion using our software and GIS. (For interpretation of the references to color in this figure legend, the reader is referred to the Web version of this article.)

Appendix A. Supplementary data

Supplementary data related to this article can be found at https://doi.org/10.1016/j.cageo.2018.07.006.

References

Abu Zeid, N., Bignardi, S., Caputo, R., Mantovani, A., Tarabusi, G., Santarato, G., 2014. Shear-wave velocity profiles across the Ferrara arc: a contribution for assessing the recent activity of blind tectonic structures. In: Proceedings of the 33th GNGTS National Convention, vol. 1. pp. 117–122.

Abu Zeid, N., Corradini, E., Bignardi, S., Santarato, G., 2016. Unusual geophysical techniques in archaeology - HVSR and induced polarization, a case history. In: 22nd European Meeting of Environmental and Engineering Geophysics, NSAG-2016https://doi.org/10.3997/2214-4609.201602027.

Abu Zeid, N., Corradini, E., Bignardi, S., Nizzo, V., Santarato, G., 2017a. The passive seismic technique 'HVSR' as a reconnaissance tool for mapping paleo-soils: the case of the Pilastri archaeological site, northern Italy. Archaeol. Prospect. https://doi.org/10.1002/arp.1568.

Abu Zeid, N., Bignardi, S., Santarato, G., Peresani, M., 2017b. Exploring the paleolithic cave of Fumane (Italy): geophysical methods as planning tool for archaeology. SEG Tech. Progr. Expand. Abstr. 2017, 5125–5129. https://doi.org/10.1190/segam2017-17729320.1.

Agostini, L., Boaga, J., Galgaro, A., Ninfo, A., 2015. HVSR technique in near-surface thermal-basin characterization: the example of the Caldiero district (North-East Italy). Environ. Earth Sci. 74 (2), 1199–1210. https://doi.org/10.1007/s12665-015-4109-0.

Aki, K., Richards, P.G., 2002. Quantitative Seismology, second ed. University Science Books, Sausalito, CA 700pp.

Albarello, D., Cesi, C., Eulilli, V., Lunedei, E., Paolucci, E., Pileggi, D., Puzzilli, L.M., 2011. The contribution of the ambient vibration prospecting in seismic microzoning: an example from the area damaged by the 26th April 2009 l'Aquila (Italy) earthquake. Bollettino di. Geofisica. Teorica ed. Applicata 52 (3), 513–538.

Albarello, D., Castellaro, S., 2011. Tecniche sismiche passive: indagini a stazione singola. Ingegneria Sismica (supplemento) XXVIII (2), 32–62 (in Italian).

Barazza, F., Malisan, P., Carniel, R., 2009. Improvement of H/V technique by rotation of the coordinate system. Commun. Nonlinear Sci. Numer. Simulat. 14 (1), 182–193. https://doi.org/10.1016/j.cnsns.2007.11.016.

Bard, P.Y., 1998. Microtremor measurement: a tool for site effect estimation? In: Proceedings: The Effects of Surface Geology on Seismic Motion, Yokohama Japan, vol. 3. pp. 1251–1279.

Ben-Menahem, A., Singh, S.J., 1981. Seismic Waves and Sources. Springer-Verlag, New York.

Bignardi, S., Fedele, F., Santarato, G., Yezzi, A., Rix, G., 2013. Surface waves in laterally heterogeneous media. J. Eng. Mech. 139 (9), 1158–1165.

Bignardi, S., Santarato, G., Abu Zeid, N., 2014. Thickness variations in layered subsurface models – effects on simulated MASW. In: 76th EAGE Conference & Exhibition, Ext. Abstract WS6¬P04, https://doi.org/10.3997/2214-4609.20140540.

Bignardi, S., Mantovani, A., Abu Zeid, N., 2016. OpenHVSR: imaging the subsurface 2D/3D elastic properties multiple HVSR modeling and inversion. Comput. Geosci. 93, 103–113. https://doi.org/10.1016/j.cageo.2016.05.009.through.

Bignardi, S., Abu Zeid, N., Corradini, E., Santarato, G., 2017. The HVSR technique from array data, speeding up mapping of paleo-surfaces and buried remains: the case of the Bronze-Age site of Pilastri (Italy). SEG Tech. Progr. Expand. Abstr. 2017, 5119–5124. https://doi.org/10.1190/segam2017-17746745.1.

Bignardi, S., 2017. The uncertainty of estimating the thickness of soft sediments with the HVSR method: a computational point of view on weak lateral variations. J. Appl. Geophys. 145C, 28–38. https://doi.org/10.1016/j.jappgeo.2017.07.017.

Bignardi, S., Fiussello, S., Yezzi, A., 2018. Free and improved computer codes for HVSR processing and inversions. In: 31st Symposium on the application of Geophysics to engineering and environmental Problems, (SAGEEP 2018), Nashville Tennessee, USA March 25–29.

Bonnefoy-Claudet, S., Cornou, C., Bard, P.Y., Cotton, F., Moczo, P., Kristek, J., Fäh, D., 2006. H/V ratio: a tool for site effects evaluation. Results from 1-D noise simulations. Geophys. J. Int. 167 (2), 827–837.

Bonnefoy-Claudet, S., Köhler, A., Cornou, C., Wathelet, M., Bard, P.Y., 2008. Effects of Love waves on microtremor H/V ratio. Bull. Seismol. Soc. Am. 98, 288–300.

Castellaro, S., Imposa, S., Barone, F., Chiavetta, F., Gresta, S., Mulargia, F., 2008. Georadar and passive seismic survey in the roman amphitheatre of catania (sicily). J. Cult. Herit. 20, 1–10.

Castellaro, S., Mulargia, F., 2009. The effect of velocity inversions on H/V. Pure Appl. Geophys. 166, 567–592.

D'Alessandro, A., Luzio, D., Martorana, R., Capizzi, P., 2016. Selection of time windows in the horizontal-to-vertical noise spectral ratio by means of cluster analysis. Bull. Seismol. Soc. Am. 106 (2), 560–574. https://doi.org/10.1785/0120150017.

D'Amico, V., Picozzi, M., Baliva, F., Albarello, D., 2008. Ambient noise measurements for preliminary site-effects characterization in the urban area of Florence, Italy. Bull. Seismol. Soc. Am. 98, 1373–1388.

D'Amico, V., Picozzi, M., Albarello, D., Naso, G., Tropenscovino, S., 2004. Quick estimates of soft sediment thicknesses from ambient noise horizontal to vertical spectral ratios: a case study in southern Italy. J. Earthq. Eng. 8 (6), 895–908. https://doi.org/10.1142/S1363246904001729.

Delgado, J., Lo'pez Casado, C., Giner, J., Estévez, A., Cuenca, A., Molina, S., 2000. Microtremors as a geophysical exploration tool: applications and limitations. Pure Appl. Geophys. 157, 1445–1462.

Gallipoli, M.R., Mucciarelli, M., Eeri, M., Gallicchio, S., Tropeano, M., Lizza, C., 2004a. Horizontal to vertical spectral ratio (HVSR) measurements in the area damaged by the 2002 molise, Italy. Earthquake. Earthq. Spectra 20 (1), 81–93. https://doi.org/10.1193/1.1766306.

Gallipoli, M.R., Mucciarelli, M., Castro, R.R., Mochavesi, G., Contri, P., 2004b. Structure, soil-structure response and effects of damage based on observations of horizontal-to-vertical spectral ratios of microtremors. Soil Dynam. Earthq. Eng. 24, 487–495.

Gallipoli, M.R., Stabile, T.A., Massolino, G., Abu Zeid, N., Chiauzzi, L., Bignardi, S., Rebez, A., Mucciarelli, M., 2018. Ambient vibration tests on a building before and after the 2012 emilia (Italy) earthquake, and after seismic retrofitting. In: 16th European Conference on Earthquake Engineering (16ECEE) June 2018, Thessaloniki, Greece.

Garcia-Jerez, A., Luzon, F., Navarro, M., Perez-Ruiz, A., 2006. Characterization of the sedimentary cover of the Zafarraya basin, southern Spain, by means of ambient noise. Bull. Seismol. Soc. Am. 96 (3), 957–967. https://doi.org/10.1785/0120050061.

Gosar, A., Lenart, A., 2010. Mapping the thickness of sediments in the Ljubljana Moor basin (Slovenia) using microtremors. Bull. Earthq. Eng. 8, 501–518. https://doi.org/10.1007/s10518-009-9115-8.

Guéguen, P., Cornou, C., Garambois, S., Banton, J., 2007. On the limitation of the H/V spectral ratio using seismic noise as an exploration tool: application to the grenoble valley (France), a small apex ratio basin. Pure Appl. Geophys. 164, 115–134. https://doi.org/10.1007/s00024-006-0151-x.

Herak, M., 2008. ModelHVSR-A Matlab tool to model horizontal-to-vertical spectral ratio of ambient noise. Comput. Geosci. 34, 1514–1526.

Herak, M., Allegretti, I., Herak, D., Kuk, K., Kuk, V., Marić, K., Markušić, S., Stipčević, J., 2010. HVSR of ambient noise in Ston (Croatia): comparison with theoretical spectra and with the damage distribution after the 1996 Ston-Slano earthquake. Bull. Earthq. Eng. 8, 483–499.

Hinzen, K.G., Scherbaum, F., Weber, B., 2004. On the resolution of H/V measurements to determine sediment thickness, a case study across a normal fault in the lower Rhine embayment, Germany. J. Earthq. Eng. 8 (6), 909–926. https://doi.org/10.1142/S136324690400178X.

Ibs-von Seht, M., Wohlenberg, J., 1999. Microtremor measurements used to map thickness of soft sediments. Bull. Seismol. Soc. Am. 89 (1), 250–259.

Kobayashi, K., 1980. A method for presuming deep ground soil structures by means of longer period microtremors. In: Proc. Of the 7th WCEE, Sept. 8-13, Istanbul Turkey, vol. 1. pp. 237–240.

Konno, K., Ohmachi, T., 1998. Ground motion characteristics estimated from spectral ratio between horizontal and vertical components of microtremors. Bull. Seismol. Soc. Am. 88 (1), 228–241.

Lunedei, E., Albarello, D., 2010. Theoretical HVSR curves from full wavefield modelling of ambient vibrations in a weakly dissipative layered Earth. Geophys. J. Int. 181, 1093–1108. https://doi.org/10.1111/j.1365-246X.2010.04560.x.

Lunedei, E., Albarello, D., 2015. Horizontal-to-vertical spectral ratios from a full-wavefield model of ambient vibrations generated by a distribution of spatially correlated surface sources. Geophys. J. Int. 201 (2), 1140–1153. https://doi.org/10.1093/gji/ggv046.

Mantovani, A., Abu-Zeid, N., Bignardi, S., Santarato, G., 2015. A geophysical transect across the central sector of the Ferrara Arc: passive seismic investigations - part II. In: Proceedings of the 34th GNGTS National Convention 1. pp. 114–120.

Mantovani, A., Valkaniotis, S., Rapti, D., Caputo, R., 2018. Mapping the palaeo-Piniada valley, central Greece, based on systematic microtremor analyses. Pure Appl. Geophys. 175 (3), 865–881. https://doi.org/10.1007/s00024-017-1731-7.

Matsushima, S., Hirokawa, T., De Martin, F., Kawase, H., Sánchez-Sesma, F.J., 2014. The effect of lateral heterogeneity on horizontal-to-vertical spectral ratio of microtremors inferred from observation and synthetics. Bull. Seismol. Soc. Am. 104 (1), 381–393. https://doi.org/10.1785/0120120321.

Motamed, R., Ghalandarzadeh, A., Tawhata, I., Tabatabaei, S.H., 2007. Seismic microzonation and damage assessment of Bam city, Southeastern Iran. J. Earthq. Eng. 11 (1), 110–132.

Mucciarelli, M., Gallipoli, M.R., 2001. A critical review of 10 years of microtremor HVSR technique. Boll. Geofis. Teor. Appl. 42, 255–266.

Nakamura, Y., 2000. Clear identification of fundamental idea of Nakamura's technique and its applications. In: Proceedings of the 12th World Conference on Earthquake Engineering, New Zealand, 8pp.

Nakamura, Y., 1989. A method for dynamic characteristics estimation of subsurface using microtremor on the ground surface. Q. Rep. 30, 25–33.

Nogoshi, M., Igarashi, T., 1970. - on the propagation characteristics of microtremors. J. Seism. Soc. Japan 23, 264–280.

Nogoshi, M., Igarashi, T., 1971. On the amplitude characteristics of microtremor (Part 2). J. Seismol. Soc. Jpn. 24, 26–40 [in Japanese].

Obradovic, M., Abu Zeid, N., Bignardi, S., Bolognesi, M., Peresani, M., Russo, P., Santarato, G., 2015. High resolution geophysical and topographical surveys for the characterization of Fumane Cave Prehistoric Site, Italy. Near Surf Geosci 2015. https://doi.org/10.3997/2214-4609.201413676.

Paolucci, E., Albarello, D., D'Amico, S., Lunedei, E., Martelli, L., Mucciarelli, M., Pileggi, D., 2015. A large scale ambient vibration survey in the area damaged by May-June 2012 seismic sequence in Emilia Romagna, Italy. Bull. Earthq. Eng. 13, 3187–3206.

Parolai, S., Bormann, P., Milkereit, C., 2002. New relationships between Vs, thickness of the sediments and resonance frequency calculated by means of H/V ratio of seismic noise for the Cologne area (Germany). Bull. Seismol. Soc. Am. 92 (6), 2521–2527.

Picozzi, M., Parolai, S., Albarello, D., 2005. Statistical analysis of noise horizontal-to-vertical spectral ratios (HVSR). Bull. Seismol. Soc. Am. 95 (5), 1779–1786. https://doi.org/10.1785/0120040152.

Sánchez-Sesma, F.J., Rodríguez, M., Iturrarán-Viveros, U., Luzón, F., Campillo, M.,

Margerin, L., García-Jerez, A., Suarez, M., Santoyo, M.A., Rodríguez-Castellanos, A., 2011. A theory for microtremor H/V spectral ratio: application for a layered medium. Geophys. J. Int. 186, 221–225. https://doi.org/10.1111/j.1365-246X.2011.05064.x.

Scherbaum, F., Hinzen, K.G., Ohrnberger, M., 2003. Determination of shallow shear wave velocity profiles in the Cologne/Germany area using ambient vibrations. Geophys. J. Int. 152, 597–612.

SESAME Project, 2004. Nature of wave field, deliverable no. D13.08, 50 pages. Available on the SESAME website. http://SESAME-FP5.obs.ujf-grenoble.fr.

SESAME Project, 2005. Guidelines for the implementation of the H/V spectral ratio technique on ambient vibrations measurements, processing and interpretation, WP12, deliverable no. D23.12, 62 pages. Available on the SESAME web site: http://SESAME-FP5.obs.ujf-grenoble.fr.

Shiono, K., Ohta, Y., Kudo, K., 1979. Observation of 1 to 5 sec microtremors and their applications to earthquake engineering, Part VI: existence of Rayleigh components. J. Seismol. Soc. Jpn. 35, 115–124.

Tsai, N.C., Housner, G.W., 1970. Calculation of surface motions of a layered half-space. Bull. Seismol. Soc. Am. 60, 1625–1651.

Wathelet, M., Jongmans, D., Ohrnberger, M., 2004. Surface wave inversion using a direct search algorithm and its application to ambient vibration measurements. Near Surf. Geophys. 2, 211–221.

Wathelet, M., 2008. An improved neighborhood algorithm: parameter conditions and dynamic scaling. Geophys. Res. Lett. 35https://doi.org/10.1029/2008GL033256. L09301.

Wilken, D., Wunderlich, T., Majchczack, B., Andersen, J., Rabbel, W., 2015. Rayleigh-wave resonance analysis: a methodological test on a Viking age pit house. J. Cult. Herit. 9, 357–366. https://doi.org/10.1002/arp.1508.

Withers, M., Aster, R., Young, C., Beiriger, J., Harris, M., Moore, S., Trujillo, J., 1998. A comparison of select trigger algorithms for automated global seismic phase and event detection. Bull. Seismol. Soc. Am. 88 (1), 95–106.